Structural Control & Health Monitoring
The Journal of the International Association for Structural Control and Monitoring

Dynamic behaviour of the carillon tower in Castel San Pietro Terme, Italy

Journal:	*Structural Control and Health Monitoring*
Manuscript ID	Draft
Wiley - Manuscript type:	Research Article
Date Submitted by the Author:	n/a
Complete List of Authors:	Azzara, Riccardo; Istituto Nazionale di Geofisica e Vulcanologia Girardi, Maria; Istituto di Scienza e Tecnologie dell'Informazione Alessandro Faedo Consiglio Nazionale delle Ricerche Padovani, Cristina; Istituto di Scienza e Tecnologie dell'Informazione Alessandro Faedo Consiglio Nazionale delle Ricerche Pellegrini, Daniele; Istituto di Scienza e Tecnologie dell'Informazione Alessandro Faedo Consiglio Nazionale delle Ricerche
Keywords:	Masonry bell towers, dynamic monitoring, bell swinging, model updating, dynamic identification

Dynamic behaviour of the carillon tower in Castel San Pietro Terme, Italy

Riccardo Mario Azzara[1], Maria Girardi[2], Cristina Padovani[2], Daniele Pellegrini[2]

[1] Istituto Nazionale di Geofisica e Vulcanologia, Osservatorio Sismologico, Arezzo, Italy

[2] Consiglio Nazionale delle Ricerche, Istituto di Scienze e Tecnologie dell'Informazione "A. Faedo", Pisa, Italy

Summary

The paper presents the experimental investigations conducted on the carillon tower of the Santissimo Crocifisso Sanctuary in Castel San Pietro (Bologna, Italy) and the analysis of data collected by velocimeters and accelerometers installed on the structure. The main goal is to assess the effects of the swinging bells on the dynamic behaviour of the tower. The paper's novelty relies on the kind of structure monitored, and the approach followed. The structure is a rare example of a carillon tower, subjected to a careful measurement campaign never carried out before. Moreover, the experimental results are complemented by numerical simulations of the dynamic behaviour of the tower subjected to the action of a swinging bell.

Keywords

Masonry bell towers, dynamic monitoring, bell swinging

1. INTRODUCTION

This paper presents the results of the experimental investigations and numerical analyses conducted on the tower of the Santissimo Crocifisso Sanctuary in Castel San Pietro, focused on assessing the effects of the swinging bells on the dynamic behaviour of the structure.
Studies on the dynamic interaction between bells and masonry towers are quite scarce. A seminal study dates back to the Seventies [1] when the first experiments were set to determine the inertia forces induced by the bell ringing. Further thorough investigations were conducted for the Millennium celebrations in England [2]. Relevant outcomes are reported in the references [3]-[14]. The papers by Bennati et al. [3], [4] present the experimental tests carried out on the bell tower of the San Miniato Cathedral, provide an analytical expression of the dynamic actions transmitted to the tower by the swinging bells and describe the motion of the tower as well. The dynamic behaviour of a bell tower in Valencia is the subject of the paper by Ivorra and Pallares [5], where possible dynamic amplification phenomena connected to the closeness of excitation and bell tower frequencies are investigated. A resonance phenomenon between the first natural frequency of a modern bell tower and some harmonic components of the dynamical actions transmitted by the swinging bells is highlighted in [6], where the authors show that this phenomenon is significantly reduced by stiffening the structure. A similar analysis on a modern concrete bell tower is also shown in [7]. The outcomes of the studies conducted on the Soncino civic tower subjected to the bells'action are reported in [8], where the model of the tower is calibrated via experimental data and the effect of retrofitting on the stress field is assessed. Another investigation on the effects produced by the bells' swinging has been carried out on the SS. Medici Bell Tower (Apulia, Italy) [9], a framed reinforced concrete structure with masonry walls. High accelerations are recorded on the bell tower. When the bells swing in the North-South direction, a coupled behaviour between the North-South and East-West deformations has been detected, explaining the presence of cracks in the structure. The interaction between the structure's natural frequencies and the forces generated by the bells is analysed in [10] for masonry bell towers, considering different bells arrangement and turning speeds along with the tower's dynamic characteristics. The dynamic behaviour of a Tuscan masonry bell tower subjected to the

forces generated by the swinging bell is addressed by [11]. A parametric analysis of the dynamic interaction between the harmonic bell forces and the fundamental tower modes is conducted, assuming swing angles, velocities, position and direction of the bells as parameters and using the dynamic amplification factor [15], under the hypothesis of linear elasticity. Vincenzi et al. [12] assess the dynamic response of a bell tower in North Italy subjected to the oscillations of swinging bells under the hypothesis of linear elasticity. The influence of swinging bells on the crack distribution in a bell tower in Lithuania is analysed in the paper [13], where the modal curvature approach is used to detect damage in the tower. Finally, Nochebuena-Mora et al. [14] investigate possible resonance effects by comparing the natural frequencies of a bell tower in Portugal and those of the bells' actions; they also present the results of nonlinear dynamic analysis in terms of displacements and cracking.

The present paper, which adopts the approaches followed in the previous papers, aims to improve the knowledge of the dynamic behaviour of masonry bell towers. The structure under examination is a challenging, complex, and never investigated case study, a carillon masonry bell tower hosting fifty-five bells, which in 2021 was instrumented by the authors to measure the velocities induced by the bells and determine the structure's dynamic properties. The carillon mechanism, which is driven by a keyboard at the tower's base, and the number and size of the bells involved represent an example of a bell tower rare in Europe and unique in Italy. The study's novelty also relies on the possibility of comparing experimental and numerical results coming from finite element dynamic analyses conducted with the NOSA-ITACA code, a freely downloadable program entirely developed by the authors (www.nosaitaca.it), both in the linear and in the nonlinear field.

The paper is organized as follows. In Section 2, we describe the tower of the Santissimo Crocifisso Sanctuary and the carillon system. Section 3 provides a detailed description of the experimental tests conducted on the tower in 2021 to assess the system's dynamic response to the action of the bells. Six experiments were carried out selectively activating the bells, to measure the tower's response induced by different vibration sources and determine the peak velocities recorded by the instruments at different heights. Two ambient vibration tests complemented the six experiments. These two tests were conducted with the bells at rest, the former before and the latter at the end of the bells' activation and allowed to determine the structure's experimental frequencies and mode shapes via Operational Modal Analysis (OMA) techniques. Section 4 is devoted to finite element (FE) simulations. A FE model of the tower is calibrated via the NOSA-ITACA code by minimizing the discrepancy between experimental and numerical frequencies. Linear and nonlinear dynamic analyses of the calibrated model subjected to the action transmitted by the biggest of the swinging bells are then conducted with NOSA-ITACA. The numerical velocities are compared with their experimental counterparts recorded in some selected points during the tests. Conclusions are drawn in Section 5.

2. THE CARILLON TOWER AND ITS FIFTY-FIVE BELLS

The main building of the Santissimo Crocifisso Sanctuary in San Pietro Terme (in Central Italy, nearby Bologna) was built in the first half of the Eighteenth century and enlarged at the beginning of the past century with the construction of the pronaos (Figure 1). In the same years (1926-1930), Giulio Gollini built the present masonry bell tower (Figure 2) and designed one of the most famous and complex bell carillons in Italy and Europe, consisting of fifty-five bells connected to a keyboard placed at the tower's base via an electro-pneumatic system. The bell tower overlooks a large public square. The music of the carillon is often employed during religious and civil ceremonies, and the local authorities organize concerts in which the sound of the carillon accompanies the civic band on the square.

The renowned *Brighenti* foundry in Bologna produced the bells hosted at different levels inside the tower. The lower bell chamber (Figure 3a), at about 15 m in height, hosts forty-eight bells hung by hammers, activated in turn by the *carillonneur* at the keyboard. These bells do not move and are suspended from a steel structure, which rests on the chamber's floor.

Figure 1. The Santissimo Crocifisso Sanctuary in San Pietro Terme (BO).

The upper bell chamber (Figure 3b), at about 18 m in height, hosts seven swinging bells: three small bells (no. 8, 9, and 10) are activated via long ropes going downward from the bell's floor to the tower's base; bell ringers swing the remaining four bells (52 to 55) in particular circumstances (Figure 4b). These four bells, suspended from a steel frame supported by the bell chamber's floor and masonry, can swing, and be also stroked by hammers. The bronze bells are balanced by wooden counterweights that allow the system to fulfil large oscillations, up to 160° from the rest position, following the Central Europe system known as "*Alla Romana*" [16]. The bells can also overturn and remain upright with their mouths up until the bell ringers push them down again (*English* system [1]). This configuration is occasionally reached at the end of the bells' concerts for very few cycles. The heaviest bell is the no. 51, with a diameter of about 1200 mm; it is located in the lower bell chamber (Figure 3a) and is struck by a hammer (Figure 4a). Among the swinging bells located in the upper chamber, the heaviest is the no. 54 (Figure 3b), with a diameter of about 880 mm. Figure 4b shows the bells swung by bell ringers during the experiments.

As far as the geometry is concerned, the tower is about 31 m high, with a square transverse section of about 5.1m x 5.1m. The masonry walls have a thickness of 0.8 m, constant for the first 15 m. Upstairs, the bell chambers' floor is supported by metallic beams and small masonry vaults. The tower ends with a dome, which takes up the last 7 m of the structure. The bell tower is adjacent to the sanctuary, whose walls can constitute a horizontal constraint for the tower for the first 4.5 m.

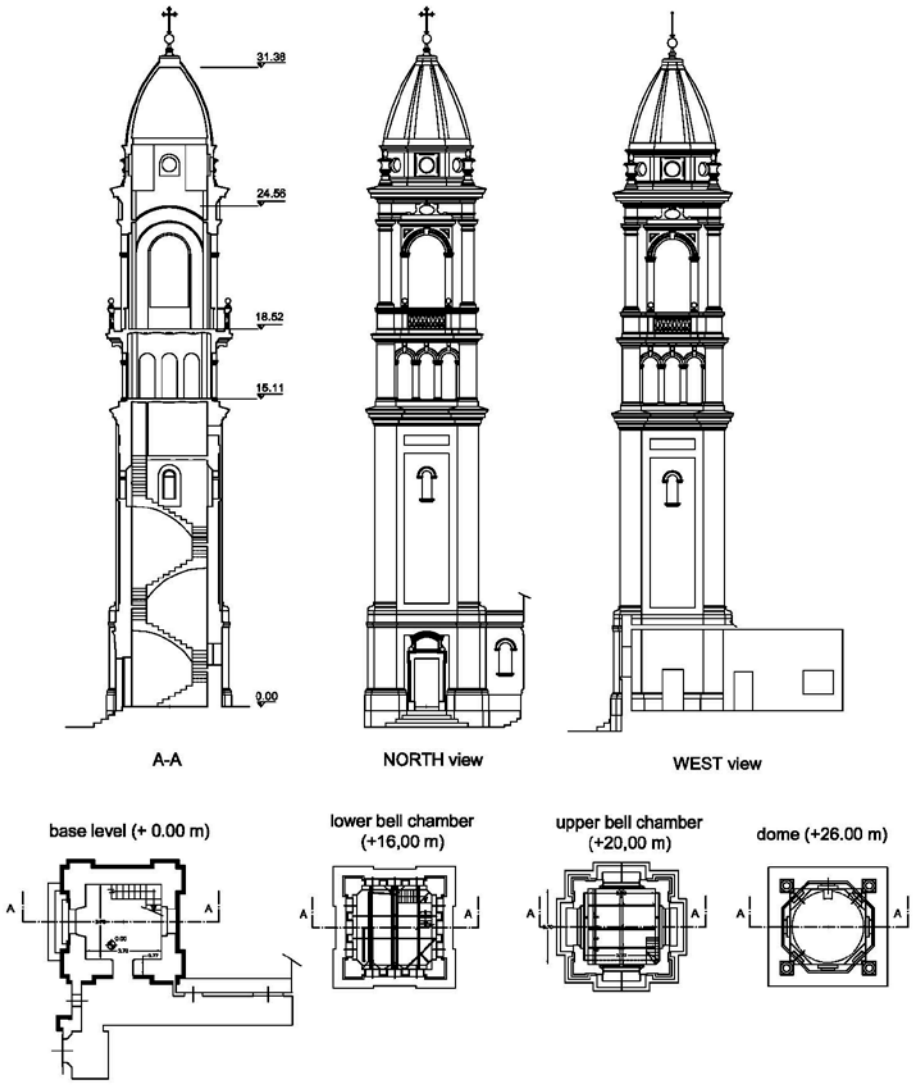

Figure 2. The bell tower of the Santissimo Crocifisso Sanctuary (by courtesy of A. Nerozzi, M. Naldi, G Dallavalle and the parish of Santa Maria Maggiore).

3. DYNAMIC MONITORING AND IDENTIFICATION

This section describes the experimental tests and analyses the data recorded by the instruments installed on the tower. The bells were activated selectively during the experiments to measure the tower's response induced by their dynamic actions. The ambient vibration tests conducted with the bells at rest allowed the dynamic identification of the tower.

3.1. Experimental tests

The authorities in charge of the Sanctuary's maintenance requested experimental investigations because of a perceived increase in the magnitude of the tower's vibrations and after a survey of the tower's structure. On 17 May 2021, the authors carried out the measurements. The instrumentation consisted of seven seismic stations produced by SARA Electronic Instruments and two triaxial accelerometers. The authors installed four SS45 (eigenfrequency 4.5 Hz) and three SS20 (eigenfrequency 2 Hz) triaxial velocimeters, each coupled with a 24-bit digitizer (SL06). The velocimeters' transfer functions allowed enlarging the frequency bandwidth, thus giving a correct

estimation of the measured velocities. The instrumental set was completed by two broadband triaxial accelerometers Guralp CMG5T coupled with two 24-bit digitizers Reftek 72A07. The sensors' arrangement is shown in Figure 5 and Figure 6. The *y* axis of all instruments coincided with the swinging direction of the bells in the upper chamber (North direction). The sampling frequency was set to 100 Hz. All stations were synchronized via GPS signal receivers.

The experiments were designed to consider different kinds of actions: vibrations induced by the only sound of the carillon, by the swinging of the major bells in case of a free or fixed clapper, by the bells' swinging and carillon acting together. In addition, some ambient vibration measurements were carried out before and after the experiments to identify the modal properties of the tower and recognize potential damage. Table 1 describes the six experiments; Experiment 0 (OMA) and Experiment 7 (OMA) denote the initial and final ambient vibration test, respectively.

Figure 7 and Figure 8 show the velocity measured by the seismic stations during Experiments 2 and 3. The swinging of the four bells in succession is evident in the signals. The velocity recorded in Experiment 3 is about three times lower than that recorded during Experiment 2 when the clappers are free to move and strike the bells.

The signals also show that when the bells' clappers are free to move (Experiment 2), the heaviest bell (bell no. 54) induces the maximum velocities, as expected. When the clappers are not allowed to play, the maximum velocity's magnitude is induced instead by bell no. 55. Visual inspection of the videos recorded during the experiment revealed that, although the bell ringers did not allow the clappers to ring, they sometimes rang anyway during the bells' oscillations. During the swaying of bell no. 55, the clapper rang four times, two times during the swaying of bells no. 52 and no. 53, while only the bell no. 54 oscillated without strokes. The clappers' strokes are, in effect, evident in the experiment's signals.

Figure 9 provides further information on the tower's behaviour over the six experiments in the band [0, 15] Hz; it shows the spectrogram of the signals recorded in the *x* and *y* directions by the sensor SS45 2897, placed in the lower bell chamber at the height of 15.10 m. The tower's natural frequencies, identified in subsection 3.2, are visible in the band [0, 9] Hz (horizontal lines). As a result of the bell swinging, the power spectral density increases in the entire band during all experiments, particularly during Experiment 5. It is worth noting that the maximum increase in the power spectral density during the experiments is visible in the band [1, 3] Hz. Figure 10 shows, for the six experiments, the velocities recorded over the time by the couples of sensors 2045 versus 2897 and 0944 versus 2896, in the *x* and *y* directions; each pair is formed of velocimeters aligned along a vertical line but placed at different quotes (Figure 5). The dashed line in each chart represents the linear regression, reported along with the squared correlation index R.

Except for Experiments 1 and 6 (carillon only), the R-values are high, indicating a good correlation between the velocities and a linear trend alongside the tower during the bell swinging. Interestingly, when the bells' clappers are not allowed to play (during Experiment 3), the R index, calculated between velocities recorded in the y-direction, increases compared to Experiment 2 for both pairs of instruments.

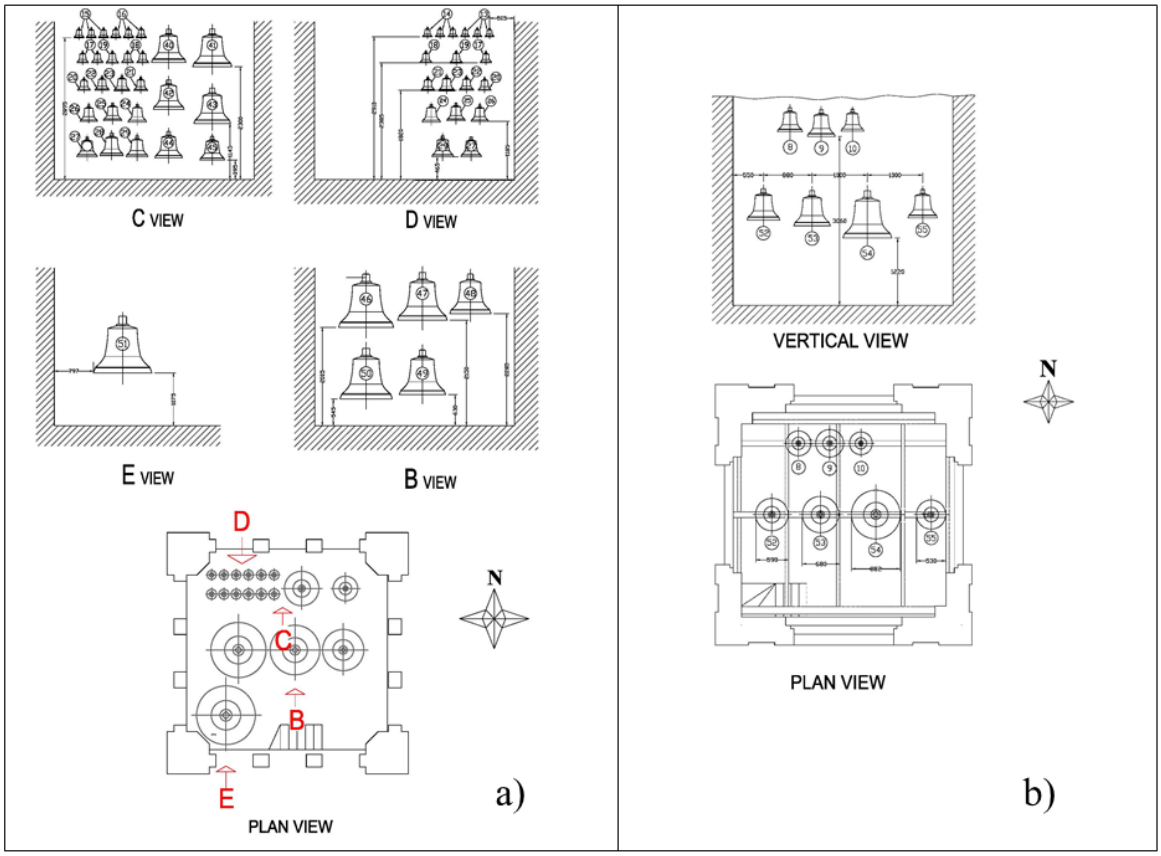

Figure 3. Arrangement of the bells in the lower (a) and in the upper (b) bell chamber (by courtesy of A. Nerozzi, M. Naldi, G Dallavalle and the parish of Santa Maria Maggiore).

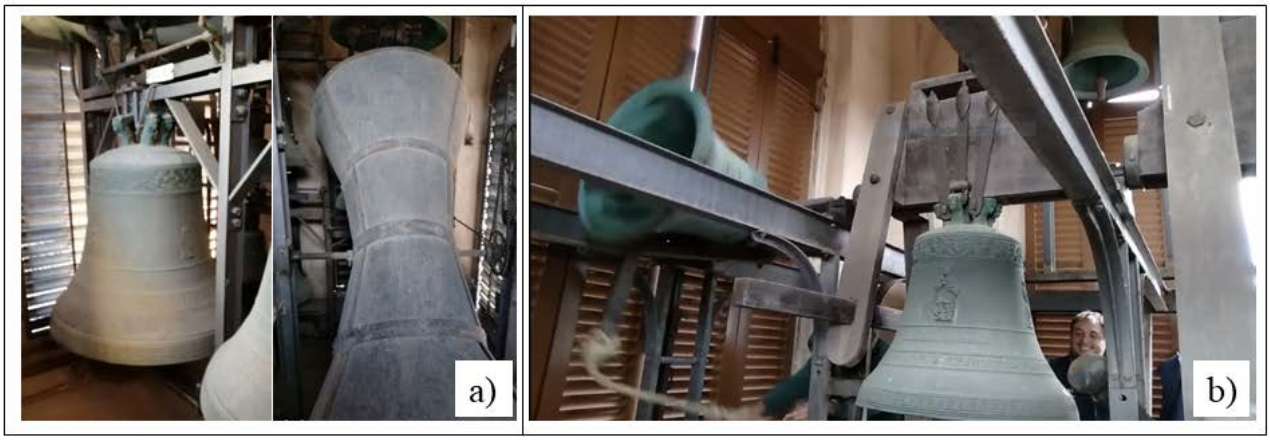

Figure 4**.** a) Some details of the bell carillon system in the lower bell chamber; b) bells in the upper bell chamber rung by the bell ringers during Experiment 3

Table 2 reports the peak component particle velocity (PCPV) recorded by the instruments during the experiments for each signal component. The components that exceed the limit value of 8 mm/s suggested for historical buildings by many technical rules [17], [18] are highlighted in bold. The PCPV values are plotted versus the tower's height in Figure 11 for the *x* and *y* components. The analysis of the previous figures and tables allows one to make the following remarks.

1. The carillon's sound (Experiments 1 and 6) can be modelled as an impulsive action on the tower and induces velocities in the order of 0.5 mm/s, both in the *x* and *y*-direction.
2. Experiments in which the bells in the upper chamber swing (Experiments from 2 to 5) produce the highest velocity values in the swinging direction (*y*). These values are more significant than those induced by the carillon alone.
3. The most robust action is induced on the tower in Experiment 5 when all the bells (carillon plus swinging bells) ring. The highest measured values are located over the vault overlooking the upper bell chamber and reach 30 mm/s.
4. Swinging of the only bell no. 54 (Experiment 2) gives velocity values (up to 20 mm/s) comparable with those induced by all the bells playing.
5. Experiment 3, in which the bells swing without clappers, induces velocity values three times lower than those measured in Experiment 2 when the clappers are free to move and strike the bell.
6. The carillon's sound (in Experiments 1 and 6) induces velocities that vary linearly with the tower's height.
7. The experiments with the bells swinging (Experiments from 2 to 5) result in a linear velocity trend alongside the tower up to the bell chamber's floor (18 m), with values in the limit of 8 mm/s. Robust amplification of the velocity is shown instead in the upper portions of the tower. This behaviour reflects the different stiffness of the bell chamber with respect to the lower tower's structure and the fact that the reaction forces induced by swinging are applied to the tower in the high section of the bell chamber. It might also indicate that nonlinear behaviour occurs in the upper part of the structure, as confirmed by the presence of cracks in the dome and the numerical outcomes.

It is worth noting that the three instruments located in the upper bell chamber (at 18 m) and the vault (at 24 m) showed some signal saturation phenomena in the *y*-direction during the most energetic Experiment 5. Based on the recorded waveforms, we can estimate in the *y*-direction a decrease of about 15% in the PCPV magnitude. Moreover, station SS45 2542 at the tower's base stopped recording during Experiment 6 and was reset during Experiment 7 (OMA).

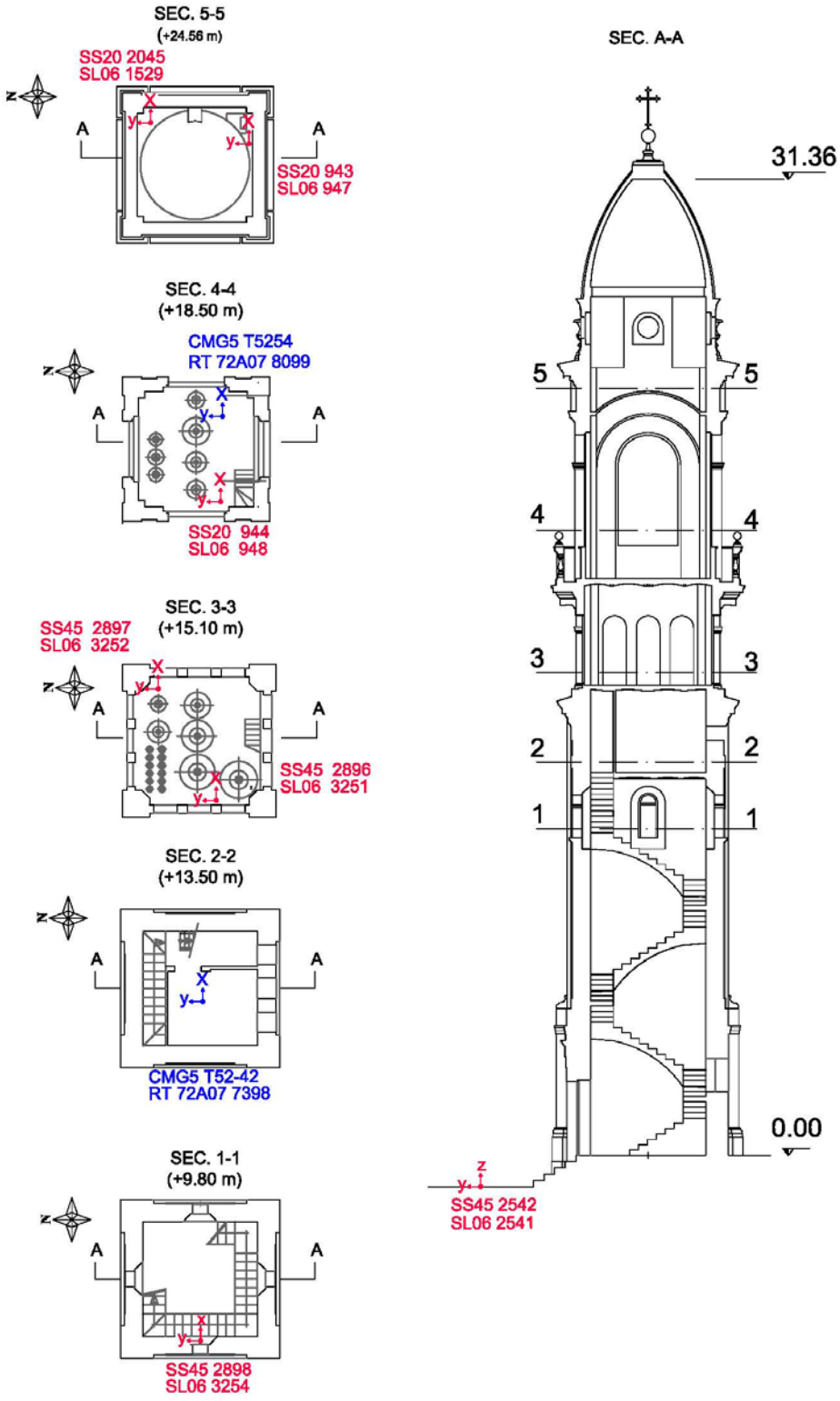

Figure 5. Sensor positions during the experiments. Seismic stations (red), accelerometers (blue).

Experiment	Duration of the experiment	Bells involved	Characteristics of the experiment	Tests conducted during the experiments
Experiment 0 (OMA)	50 minutes	None	Ambient vibration test (without bells)	

Experiment 1	9 minutes	Bells in the lower chamber (carillon)	Vibrations induced by the **carillon only**. After the activation of the electro-pneumatic system, the bells, connected to the keyboard, are hung together by the hammers.	The impulsive action is repeated for three times: TEST 1_1 TEST 1_2 TEST 1_3
Experiment 2	10 minutes	Bells in the upper chamber (swinging bells)	The major bells in the upper bell chamber are swung individually by four bell ringers.	TEST 2_1: bell no. 55 TEST 2_2: bell no. 52 TEST 2_3: bell no. 53 TEST 2_4: bell no. 54
Experiment 3	10 minutes	Bells in the upper chamber (swinging bells, fixed clappers)	The major bells in the upper bell chamber are swung individually by four bell ringers. The bells' **clappers are not allowed to play** during the experiment.	TEST 3_1: bell no. 55 TEST 3_2: bell no. 52 TEST 3_3: bell no. 53 TEST 3_4: bell no. 54
Experiment 4	12 minutes	Bells in the upper chamber (swinging bells)	Bells no. 52, 53, 54, 55 are swung together	
Experiment 5	12 minutes	Bells in the upper chamber (swinging bells) + Bells in the lower chamber (carillon)	Bells no. 52, 53, 54, 55 are swung as for the Experiment 4, together with the carillon.	
Experiment 6	5 minutes	Bells in the lower chamber (carillon)	Vibrations induced by the **carillon only**	
Experiment 7 (OMA)	25 minutes	None	Ambient vibration test (without bells)	

Table 1**.** Experiments conducted on the bell tower.

Figure 6**.** A seismic station (on the left) and an accelerometer installed on the bell tower.

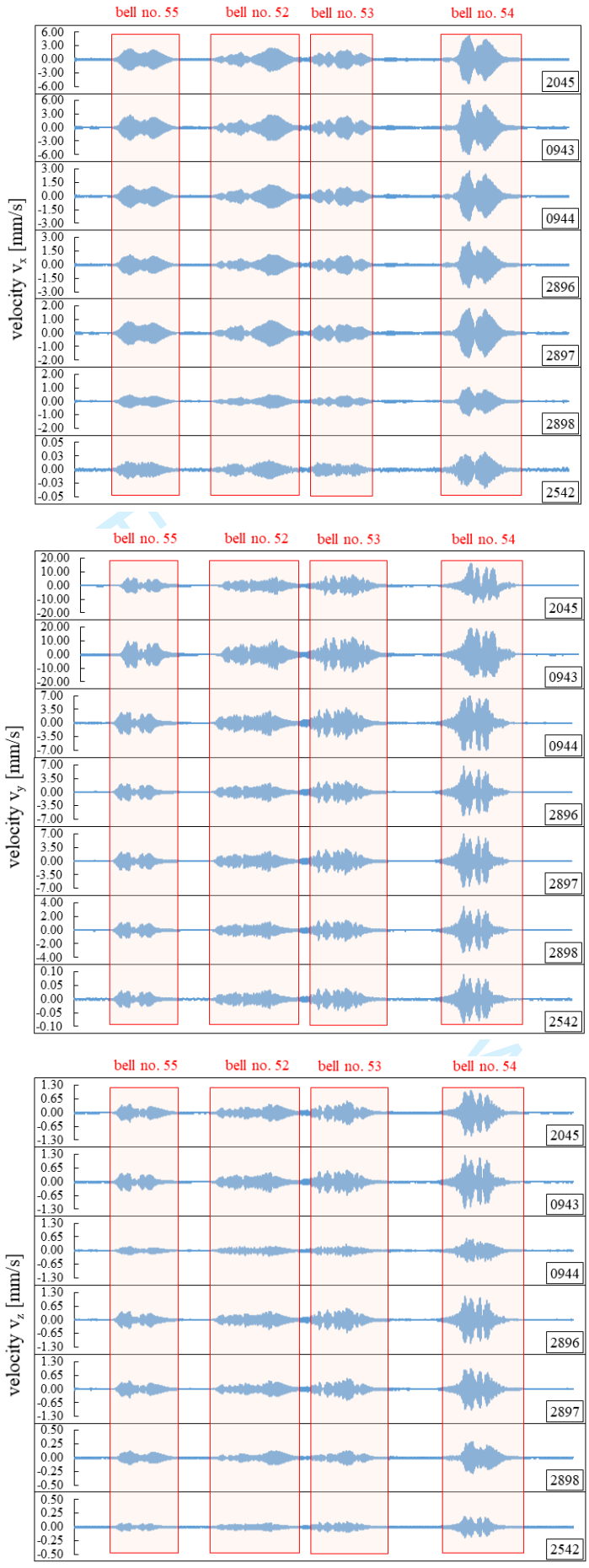

Figure 7. Velocities recorded by the seismic stations during Experiment 2.

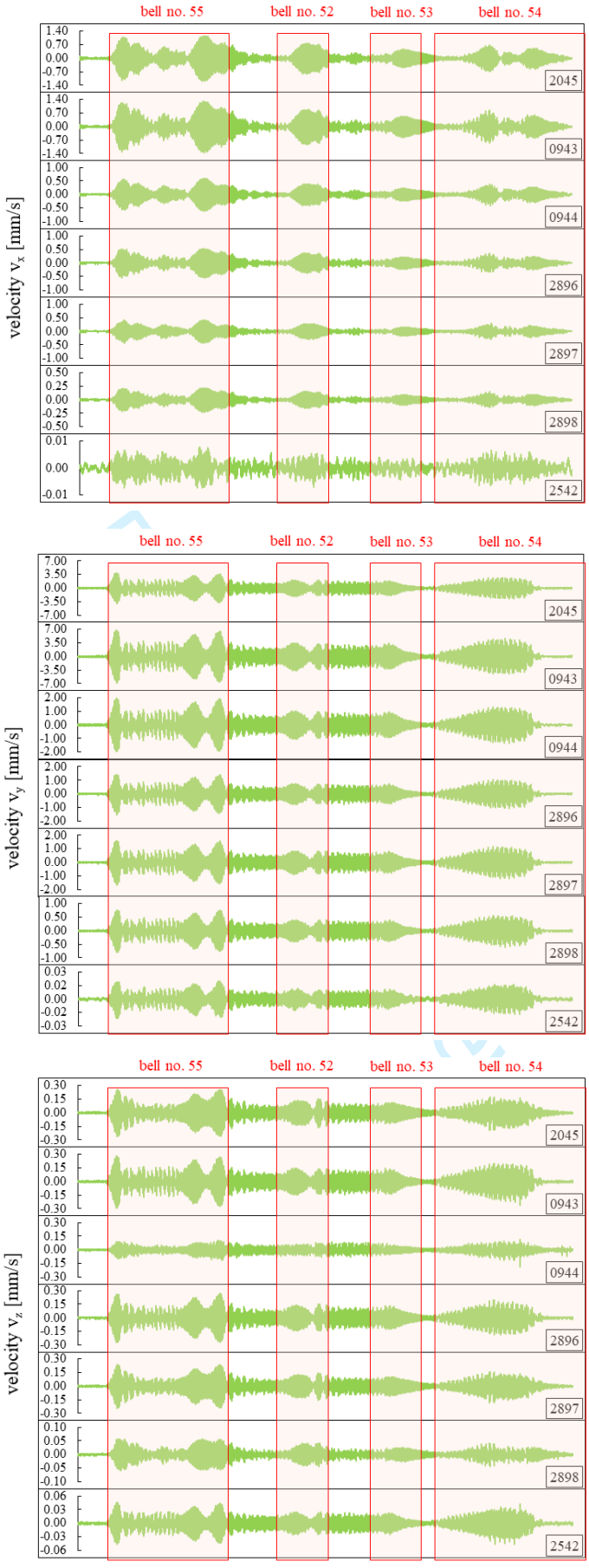

Figure 8. Velocities recorded by the seismic stations during Experiment 3.

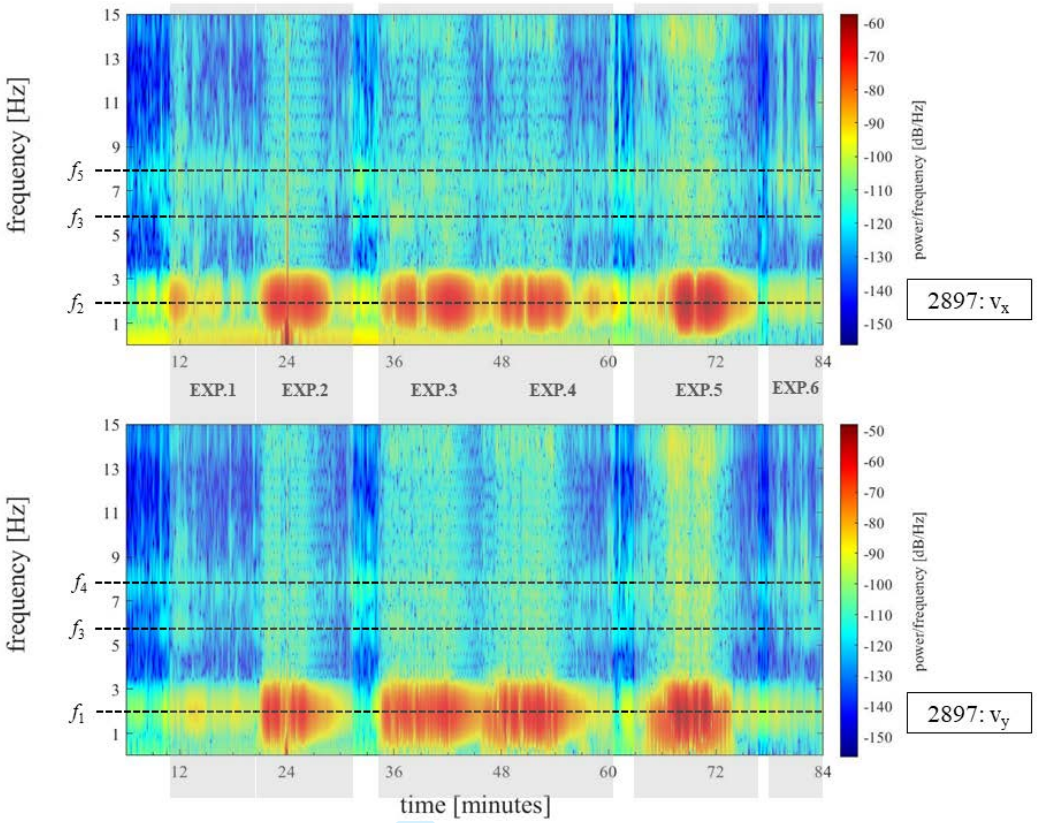

Figure 9. Spectrogram of the signal recorded by SS45 2897 (+15.10m) in the *x* (upper) and *y* (lower) directions during the experiments 1 - 6.

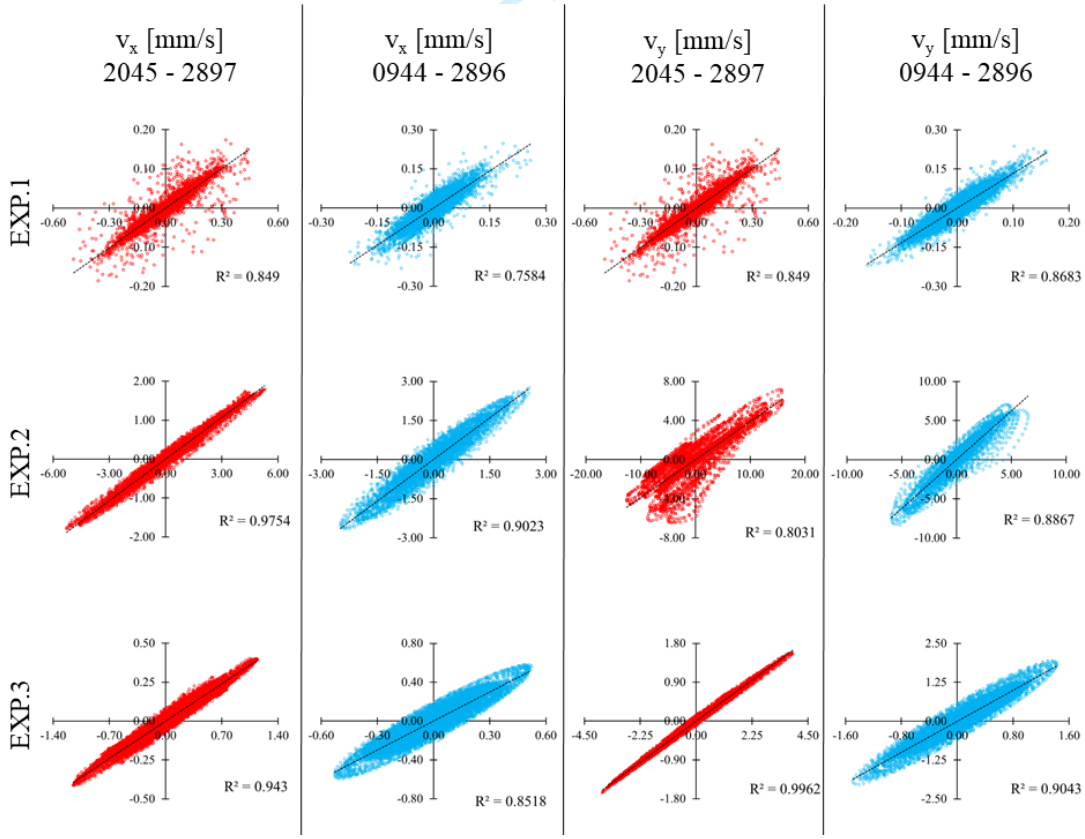

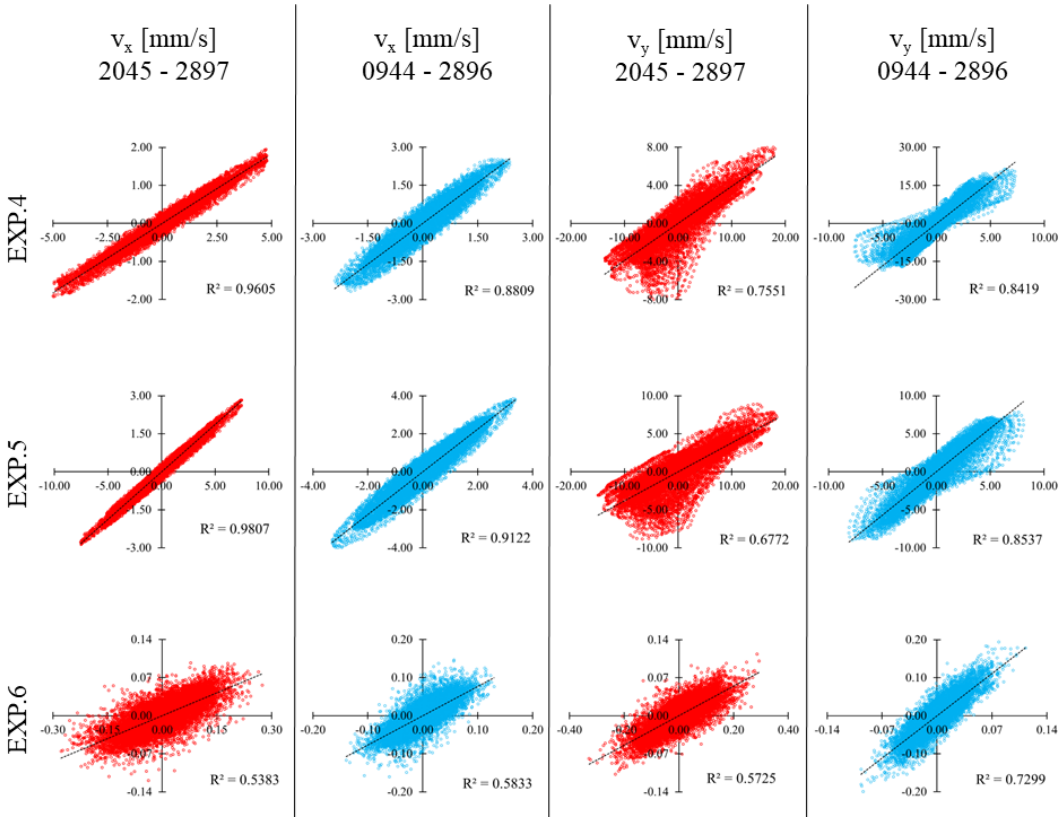

Figure 10. Correlation between velocities recorded, in the *x* and *y* directions, by sensors 2045 and 2897 (red) and by sensors 0944 and 2896 (blue).

		Experiment 1			**Experiment 2**		
Sensor ID	Level [m]	max $\|v_x\|$ [mm/s]	max $\|v_y\|$ [mm/s]	max $\|v_z\|$ [mm/s]	max $\|v_x\|$ [mm/s]	max $\|v_y\|$ [mm/s]	max $\|v_z\|$ [mm/s]
SS45 2542	0	0.008	0.004	0.01	0.03	0.09	0.19
SS45 2898	9.84	0.12	0.10	0.03	1.03	3.45	0.29
SS45 2897	15.11	0.17	0.18	0.06	1.79	7.17	0.98
SS45 2896	15.11	0.26	0.16	0.05	2.55	6.53	1.13
SS45 0944	18.52	0.25	0.24	0.13	2.75	7.06	0.58
SS20 2045	24.56	0.48	0.72	0.08	5.27	**15.91**	1.04
SS20 0943	24.56	0.59	0.41	0.14	6.24	**19.44**	1.23
		Experiment 3			**Experiment 4**		
Sensor ID	Level [m]	max $\|v_x\|$ [mm/s]	max $\|v_y\|$ [mm/s]	max $\|v_z\|$ [mm/s]	max $\|v_x\|$ [mm/s]	max $\|v_y\|$ [mm/s]	max $\|v_z\|$ [mm/s]
SS45 2542	0	0.008	0.02	0.05	0.04	0.11	0.23
SS45 2898	9.84	0.21	0.76	0.06	0.95	3.96	0.28
SS45 2897	15.11	0.40	1.58	0.24	1.95	8.00	1.14
SS45 2896	15.11	0.52	1.42	0.27	2.37	7.28	1.30
SS45 0944	18.52	0.58	1.94	0.11	2.53	7.55	0.68
SS20 2045	24.56	1.13	3.85	0.25	4.75	**18.07**	1.18
SS20 0943	24.56	1.30	6.79	0.28	5.83	**21.46**	1.44
		Experiment 5			**Experiment 6**		
Sensor ID	Level [m]	max $\|v_x\|$ [mm/s]	max $\|v_y\|$ [mm/s]	max $\|v_z\|$ [mm/s]	max $\|v_x\|$ [mm/s]	max $\|v_y\|$ [mm/s]	max $\|v_z\|$ [mm/s]
SS45 2542	0	0.05	0.11	0.24	0.08	0.08	0.03
SS45 2898	9.84	1.41	4.34	0.37	0.10	0.11	0.06
SS45 2897	15.11	2.83	8.89	1.22	0.13	0.11	0.04

SS45 2896	15.11	3.36	8.10	1.45	0.15	0.19	0.27
SS45 0944	18.52	3.85	7.81	0.87	0.29	0.30	0.09
SS20 2045	24.56	7.42	**18.28**	1.31	0.26	0.35	0.10
SS20 0943	24.56	8.17	**29.49**	1.57	0.08	0.08	0.03

Table 2. Values of the PCPV measured during the experiments.

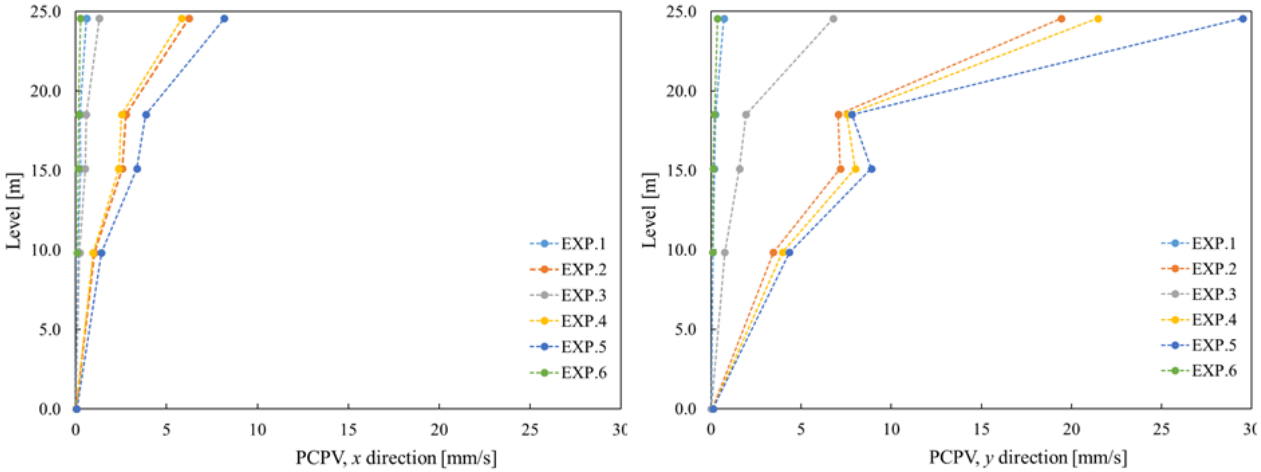

Figure 11. PCPV vs the tower's height for the six experiments, *x* (right) and *y* (left) components.

3.2. Dynamic identification of the tower

The dynamic identification of the tower is performed employing the ambient vibration measurements (Experiment 0 and 7, Table 1) carried out before and after the experiments involving the bells and carillon. All data are processed by the Covariance Driven Stochastic Subspace Identification method (SSI-cov) [19] implemented in the MACEC 3.4 toolbox [20]. Both OMA experiments are characterized by a time window longer than 2000 times T_1, where T_1 = 0.513 s is the structure fundamental period assessed on site by a Fast Fourier Transform of the signals from an instrument placed at the tower top.

Table 3 shows the value of the first six frequencies *f* identified for Experiments 0 and 7, together with the corresponding damping ratios ξ and the Modal Phase Collinearity (MPC) values. MPC is a parameter variable between 0 and 1 characterizing the "complexity" of an eigenvector; MPC is equal to 1 for real eigenvectors [21].

The last two columns of the table show the relative differences Δ of the frequencies gathered by Experiments 0 and 7 and the Modal Assurance Criterion value (MAC) [19], calculated between the mode shapes ϕ_0 extracted from the Experiment 0 and the corresponding ϕ_7 of Experiment 7.

Figure 12 shows the experimental mode shapes. The first two represent bending modes along the *y* and *x*-directions. The third and sixth are torsional mode shapes. The fourth is a bending mode shape along the diagonal direction of the cross-section of the bell tower; finally, the fifth mode is a bending in the *x*-direction.

	OMA Experiment 0			**OMA Experiment 7**			**$\Delta = (f_0-f_7)/f_7$**	**MAC**
Mode	*f* [Hz]	ξ [%]	MPC	*f* [Hz]	ξ [%]	MPC	[%]	**(ϕ_0, ϕ_7)**
1	1.951	0.94	0.99	1.930	1.00	0.97	1.08	0.98
2	1.982	0.94	0.99	1.975	0.77	0.99	0.35	0.98
3	5.881	0.53	0.99	---	---	---	---	---

4	7.545	2.57	0.98	7.544	3.48	0.99	0.01	0.98
5	7.750	3.02	0.99	7.719	2.77	0.94	0.40	0.97
6	14.453	1.64	0.98	14.356	1.51	0.91	0.67	0.97

Table 3. Dynamic properties of the bell tower obtained from OMA Experiments 0 and 7.

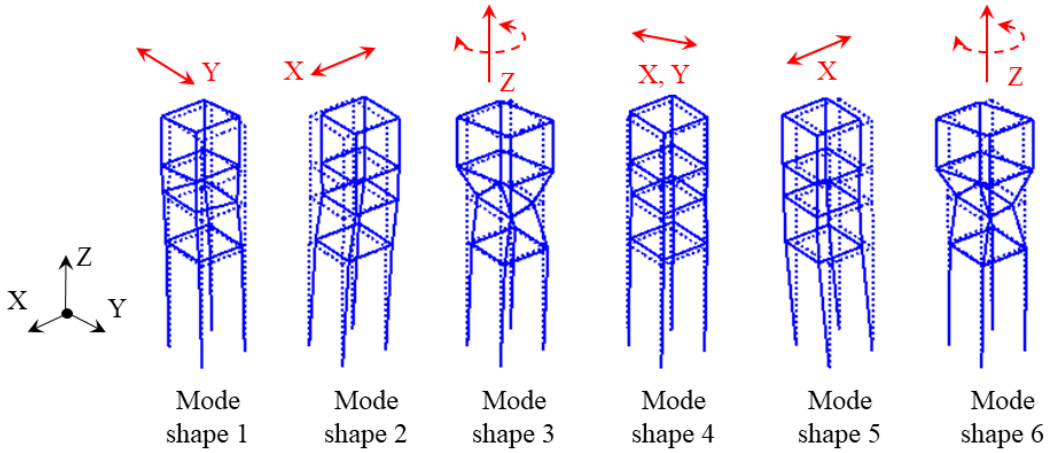

Figure 12. Experimental mode shapes.

Some remarks follow from the results reported in Table 3:

1. the maximum value of Δ is about 1.0% and has the same order of the parameter assumed by the MACEC code for clustering the frequencies in the stabilization diagram.
2. OMA Experiment 7 was carried out immediately after the experiments involving the bells and carillon, thus the input acting on the bell tower could not fully satisfy the assumption of white noise signal, which is the fundamental hypothesis underlying the OMA techniques.
3. There are no significant changes in mode shapes, being the MAC values greater than or equal to 0.97.
4. There are no significant variations in the MPC values [22].

Therefore, it follows that the slight variation in the bell tower's frequencies may likely be attributed to the choice of the clustering parameters and to modelling uncertainties and cannot be associated with any structural damage caused by the bells drive.

4. NUMERICAL SIMULATIONS

This section is devoted to calibrating the finite element model of the tower and simulating its dynamic behaviour when subjected to the action of the biggest of the swimming bells.
To this aim, by following the approach described in numerous papers [10], [8], [9],[11], [14] the FE model of the tower is subjected to the time-varying force transmitted by the bell and modelled via the approximated formulation proposed in [15]. A nonlinear dynamic analysis is conducted with the NOSA-ITACA code by assuming that the masonry materials constituting the tower have zero tensile strength and infinite compressive strength [27]. The velocities recorded in some selected points by the seismic stations installed on the tower are compared with the numerical velocities calculated by the code. For the sake of comparison, the results for the linear elastic case are also provided.

4.1. FE model updating

A refined FE model of the tower was created with NOSA-ITACA (www.nosaitaca.it/software), a software developed by ISTI-CNR for the analysis and calibration of masonry structures. The mesh of the tower, shown in Figure 13, consists of 67,747 isoparametric eight-node brick and beams elements (element no. 8 and no. 9 of the NOSA-ITACA library) with 81,777 nodes, for a total of 245,331 degrees of freedom. Beams are used to model the steel elements supporting the bells. The tower is assumed to be clamped at the base, and the presence of the adjacent sanctuary is considered via fixed constraints, up to a height of about 4.5m on the southwest side.

The global optimization algorithm implemented in NOSA-ITACA code and described in [23] is employed to calibrate the tower's numerical model. The calibration is obtained by considering the first five frequencies inferred by Experiment 0 only. In fact, in Experiment 7 the third frequency is not identified, and calculation of the remaining dynamic features could be influenced by the oscillations induced on the tower by previous Experiment 6. The choice to exclude the sixth frequency identified in the Experiment 0 from the model updating process is justified by the high degree of uncertainty affecting this quantity and the corresponding mode shape.

For the purpose of calibration, the FE model is subdivided in four sets of materials with different Young's moduli E_1, E_2, E_3 and E_4, as shown in Figure 13. The sets coincide with the higher portion of the tower including dome, drum, and bell chamber (E_4); the tower's internal slabs (E_3); the lower portion of the structure (E_1), and finally the portion included between the lower bell chamber and the tower bottom (E_2). The elastic moduli E_1, E_2, E_4, have been allowed to vary within the interval [1.0, 8.0] GPa, while E_3 ranges within [1.0, 15.0] GPa, in consideration of the different construction techniques and material used for the slabs. The mass density and the Poisson's ratio of all materials are fixed at 1800 kg/m^3 and at 0.2, respectively; the bells mass is uniformly distributed at the lower and upper bell chambers level.

Table 4 reports the optimal Young's moduli values recovered by the NOSA-ITACA code. Furthermore, the table shows, for each optimal value, the parameters ζ and η calculated by NOSA-ITACA using the Jacobian of the numerical frequencies (f_{num1}, f_{num2}, f_{num3}, f_{num4}, f_{num5}) with respect to (E_1, E_2, E_3, E_4), calculated at the minimum point. The parameters ζ and η allow to assess if the optimal parameters obtained are well-defined and robust against perturbations in the experimental data due to noise [23]. If the indices satisfy the inequalities $0 << \eta << \zeta$, then the optimal values recovered are reliably determined from the experimental measurements, even if subjected to noise (as it happens for E_1, E_2, E_4). The condition $\eta << \zeta << 1$ (occurring for the parameter E_3 of the slabs) means that the optimal value obtained cannot be reliably determined.

The table also reports the ζ^{-1} and η^{-1} quantities, which estimate the minimum and maximum percentage error in the assessment of the parameters' optimal values, under the hypothesis of a 1% error in the identification of the experimental frequencies [23]. The table shows that, in the worst-case scenario, the estimated parameters E_1, E_2, E_4 will be affected, at most, by a 9.2% error (E_1). This high percentage error can be justified by the uncertainties on the boundary conditions adopted to simulate the connection between the tower and the sanctuary. In the absence of accurate knowledge, this connection was modelled with discontinuous constraints in some nodes of the FE model. The same justification applies to the relatively high value of the Young's modulus E_1 recovered. Concerning the slabs' elastic modulus (E_3), a so high percentage error means that this parameter cannot be reliably estimated, and it does not influence the frequencies, as proved by the results of the subsequent sensitivity analysis as well.

Young modulus	Optimal value [GPa]	ζ	η	ζ^{-1}	η^{-1}
E_1	5.600	0.2157	0.1087	4.6361	9.1966
E_2	2.780	0.6689	0.5466	1.4950	1.8395
E_3	1.014	0.1433	0.0129	6.9784	77.5194
E_4	3.470	0.5085	0.4013	1.9666	2.4914

Table 4. Optimal Young's moduli values calculated by NOSA-ITACA.

Table 5 summarizes the numerical frequencies of the tower corresponding to the optimal Young's moduli and their relative error $|\Delta f|$ with respect to the experimental counterparts. The maximum value of the relative error is 0.10% (for the first two frequencies). Figure 14 shows the numerical mode shapes calculated by NOSA-ITACA at the optimal point (E_1, E_2, E_3, E_4).

Mode	f_{exp} [Hz]	f_{num} [Hz]	$\|\Delta f\|$ [%]
1	1.951	1.949	0.10
2	1.982	1.984	0.10
3	5.881	5.881	0.00
4	7.545	7.551	0.08
5	7.750	7.744	0.08

Table 5. Experimental frequencies f_{exp} and numerical frequencies f_{num} calculated by NOSA-ITACA at the optimal point (E_1, E_2, E_3, E_4).

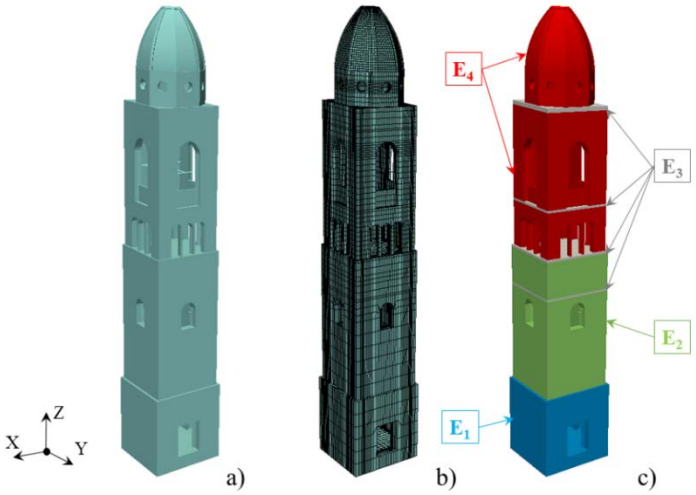

Figure 13. Model created by NOSA-ITACA code: a) geometric model; b) FE mesh; c) material sets for FE model updating

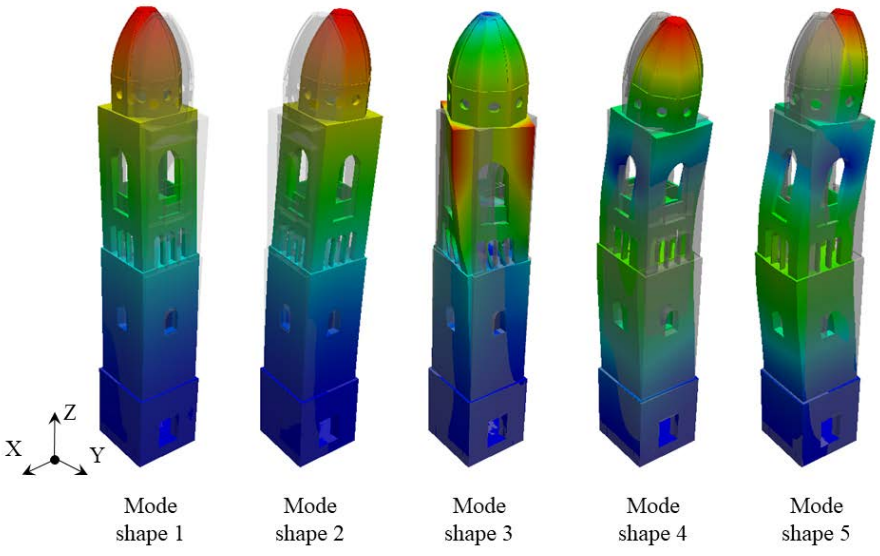

Figure 14. The five numerical mode shapes calculated by NOSA-ITACA

To investigate how variation of the Young's moduli could influence the numerical frequencies, justify the choices made in the calibration described above and thereby highlight the effectiveness and reliability of the sensitivity analysis implemented in NOSA–ITACA, a Global Sensitivity Analysis (GSA) has been carried out. Sensitivity analysis is generally performed to choose the number of updating parameters and exclude some uncertain parameters from the model updating process. In this case, we use sensitivity analysis to highlight the potentialities of the NOSA-ITACA code, which allows estimating, with reduced computational costs, both the optimal values of the unknown parameters and their reliability, thus effectively guiding the user through the model updating process. To this aim, the FE model is subdivided into six sets of materials with different Young's moduli (from E_1 to E_6, as shown in Figure 15), assuming that no information about the materials' mechanical properties is available.

The GSA has been executed through the SAFE Toolbox [24], linked to simulation models running in the NOSA-ITACA code. The Elementary Effects Test (EET method, [25]) is used to evaluate the sensitivity indices, assuming that the Young's moduli of the six materials shown in the Figure 15 have a uniform probability distribution function, and adopting the Latin Hypercube method [26] as sampling strategy. From Figure 15, where the sensitivity indices calculated via the EET method are plotted, it is possible to deduce that the Young's moduli of materials 1, 2 and 4 affect the numerical frequencies much more than the remaining parameters. These results confirm substantially the information recovered by the quantities ζ and η calculated by NOSA–ITACA and reported in Table 4 and justify the choice of considering only four parameters instead of six. It is also worth noting that the computational cost of such a global sensitivity analysis is very high (Figure 15 is the results of 560 FE modal analysis runs) with respect to the cost of the optimization procedure implemented in NOSA-ITACA, which provides both the global minimum point and an assessment of its reliability after 7 runs.

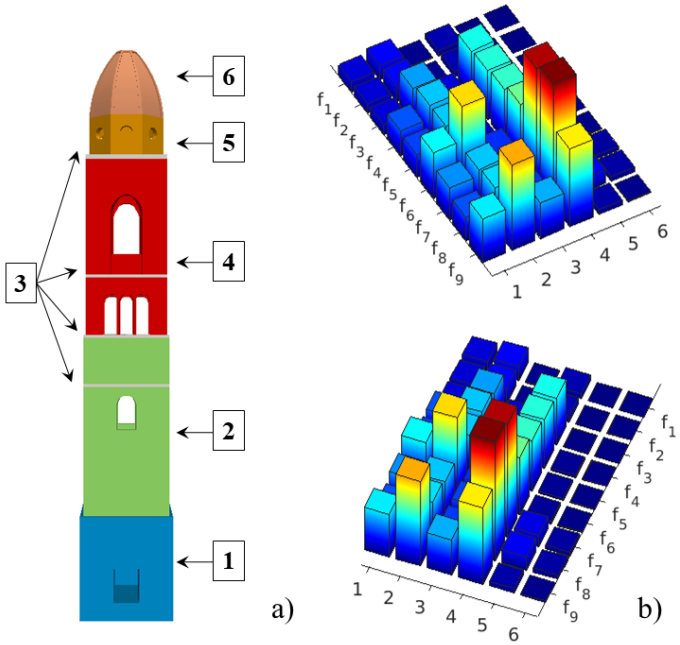

Figure 15. a) Different materials selected for the global sensitivity analysis; b) EET sensitivity indices for the first nine frequencies and six Young's moduli.

4.2. Dynamic analysis

Since the experimental tests described in Section 2 did not directly measure the bells' oscillations, the action of the bells has been assessed adopting an empirical approach. Once the geometry of the bells is known, the approximated formulation proposed in [15] can be applied and allows to estimate

the reaction forces transmitted by the bells to the supports during the swimming. In particular, the quantities of interest are the maximum amplitude of the reaction forces and their frequency content. A comparison of the frequencies of the bells' oscillations and the natural frequencies of the tower may highlight possible resonance phenomena.

The analysis is applied to bell no. 54, the heaviest swinging bell. The geometry of the bell can be deduced, once the mouth's diameter D is known, as a function of the "module" m = D/15. The bell note is also a function of D. The diameter of the bell's transverse sections varies from D (mouth) to D/2 (top), and it is worth noting that this interval corresponds to the extension of a complete octave and produces the typical timbre of the bell sound. The diameter D of bell no. 54 is 882 mm and corresponds to *La3*. In the absence of a detailed geometrical survey, the geometry of the wooden counterweight has only been estimated herein. Table 6 reports the main features of the oscillating system sketched in Figure 16, with reference to [15]. In the table *m* represents the system's mass, the unbalance *s* measures the distance of the centre of gravity to the rotation axis, *Os* is the mass moment of inertia, evaluated with respect to an axis parallel to the rotation axis and passing across the centre of gravity. The shape coefficient *c* is thus defined as

$$c = \frac{m\, s^2}{Os + m\, s^2}$$

	Bronze bell	**Wooden counterweight**	**Bell and counterweight**
Mass *m* [Kg]	380	60	440
Unbalance *s* [m]	-0.5	0.23	-0.4
Moment of inertia O_s [kg m^2]	25	0.76	52
Shape coefficient *c*	0.79	---	0.58

Table 6. Geometrical features of bell no. 54.

The quantities in Table 6 are evaluated for the bronze bell, the wooden counterweight, and the global system. The effect of the counterweight on the global system's unbalance is highlighted in the table.

The features of the bell's oscillation were deduced by inspection of some videos filmed during the experiments and some other liturgical ceremonies, having in mind [15]. The swinging effects over the tower's structure strongly depend on the maximum angle α reached by the system with respect to the vertical line during the oscillation. We investigated the effects of different values of α, from 66° suggested by [14] for wholly unbalanced systems (bronze bell only) to 160°, which has been detected by videos inspection. As reported in similar case studies [3], [11], the axial stiffness of the tower is much greater than the bending stiffness; the problem is therefore governed by the horizontal reaction

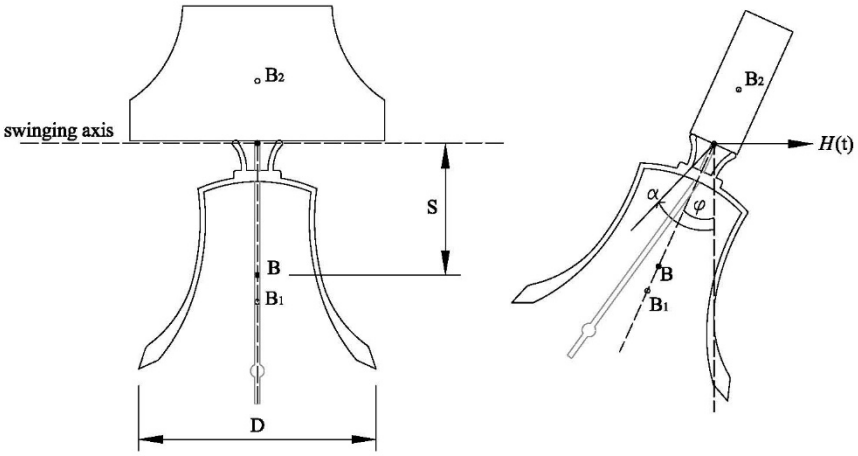

Figure 16. Scheme of bell 54 [15].

force H(t) transmitted by the swimming bell to the tower's structure. The approximated formula given by [15] for H(t) reads

$$H(t) = c\ G \sum_{n=1}^{3,5,7..} \gamma_n\,(\alpha)\ \sin\,(n\,\Omega\,t),$$

with G the weight (N) of the system and Ω the swing velocity (rad/s). The equation proposed in [14] approximates $H(t)$ using the odd terms of a Fourier series, with the fundamental frequency Ω related to the number of the bell revolutions per minute. The larger is α, the greater the super-harmonic terms contribution. Figure 17 shows the Fast Fourier Transform of function $H(t)$ for different maximum angle α values. The dashed red line indicates the fundamental frequency of the tower, which corresponds to the bending mode in the swinging direction of the bell. When the swinging angle increases, the contribution of the super-harmonic terms goes closer to the fundamental frequency, which is about 23% higher than the third-order harmonic term and 20% lower than the fifth term. It is worth noting from Figure 17 that the frequencies that give the main contribution to harmonic spectrum of H(t) are in the range [1, 3] Hz, in agreement with the experimental behaviour detected in Figure 9. The maximum amplitude of $H(t)$ also depends on α. The maximum of function H/G, plotted in Figure 18 for $\alpha = 90°$ could represent a dynamic amplification factor of the bell's weight; and it is substantially in agreement with those suggested in [28], where a simplified method is proposed based on equivalent static analysis and an amplification factor of 1.55 is reported. It is worth noting, however, that the static analysis does not allow considering the interaction between the frequency content of the force induced by the swimming bells and the dynamic properties of the tower.

Max angle α°	Rev/min	Swing velocity Ω (rad/s)	γ_1	γ_3	γ_5	γ_7	γ_9	γ_{11}
66	31	3.24	0.82	0.5	0.07	0	0	0
90	31	3.24	0.8	1	0.2	0.02	0	0
120	29	3.03	0.6	1.5	0.6	0.15	0.03	0
160	29	3.03	0.2	1.2	1.2	0.65	0.3	0.1

Table 7. Coefficients $\gamma_n\,(\alpha)$ for different values of the maximum angle α.

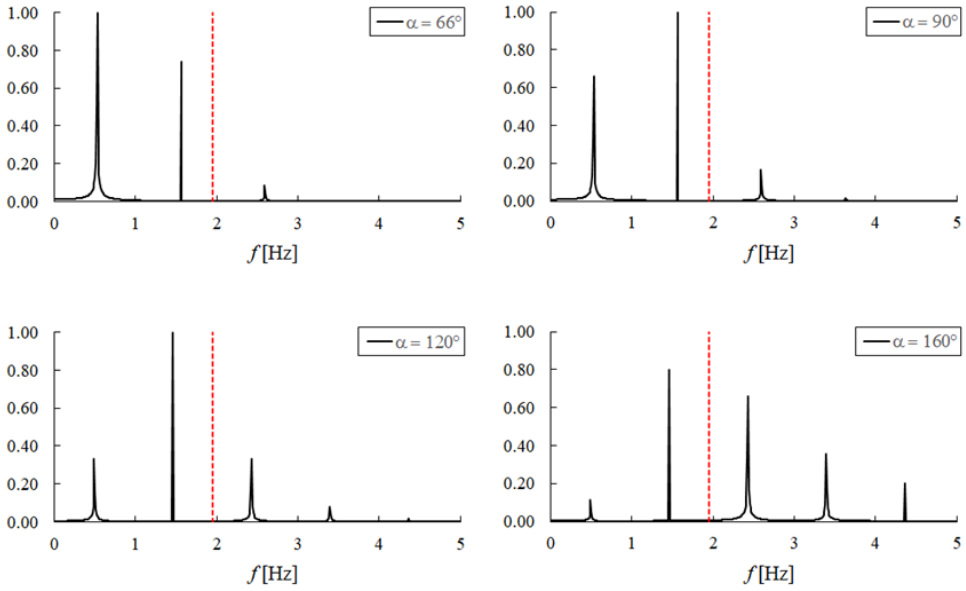

Figure 17. FFT (amplitude normalized to maximum) of function *H(t)* computed for different angles *α*. From top-left and clockwise, α = 66°, α = 90°, α = 160°, α = 120°. The red dashed line represents the fundamental frequency of the tower.

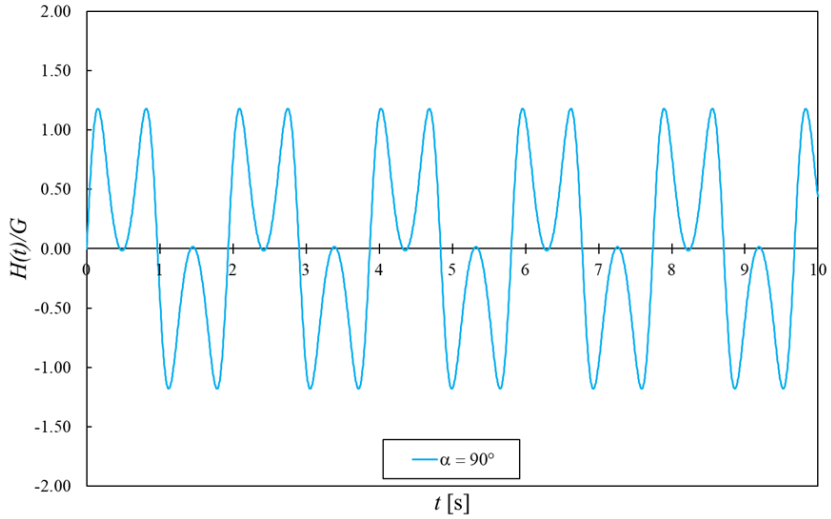

Figure 18. Function *H(t)/G* for α = 90°. The figure is plotted for *c* = 0.79.

The numerical model calibrated above has been subjected to the dynamic action *H*(t) plotted in Figure 18, and the numerical results compared with the experimental ones. The nonlinear behaviour of the tower is modelled by adopting the constitutive equation of *masonry-like* materials, implemented in NOSA-ITACA, which models masonry as an isotropic nonlinear elastic materials with zero tensile strength and infinite compressive strength. Assumptions underlying the model are that the infinitesimal strain tensor **E** is the sum of an elastic part $\mathbf{E}^e$, and a fracture part $\mathbf{E}^f$, and that the stress tensor **T** depends linearly and isotropically on the elastic part. The fracture strain is positive semidefinite and satisfies suitable orthogonality conditions involving the stress, which turns out to be a nonlinear function of the infinitesimal strain [27]. Results of the nonlinear analysis are finally compared with those obtained via classical linear analysis.

Before applying *H*(t) to the model, a nonlinear static analysis considering the self-weight only has been performed, obtaining the results summarized below and shown in Figure 19:

- the maximum value of the stress vertical component σ_{zz} is relatively low if compared to the values of compressive strength reported in the literature for masonry, and this justifies the use of a masonry-like material with infinite compression strength;
- the model is able to catch the crack pattern in the tower's dome;
- the fracture strains in the lower part of the tower's mesh can be attributed to the constrains applied to the model (no apparent cracks are visible in the actual masonry structure).

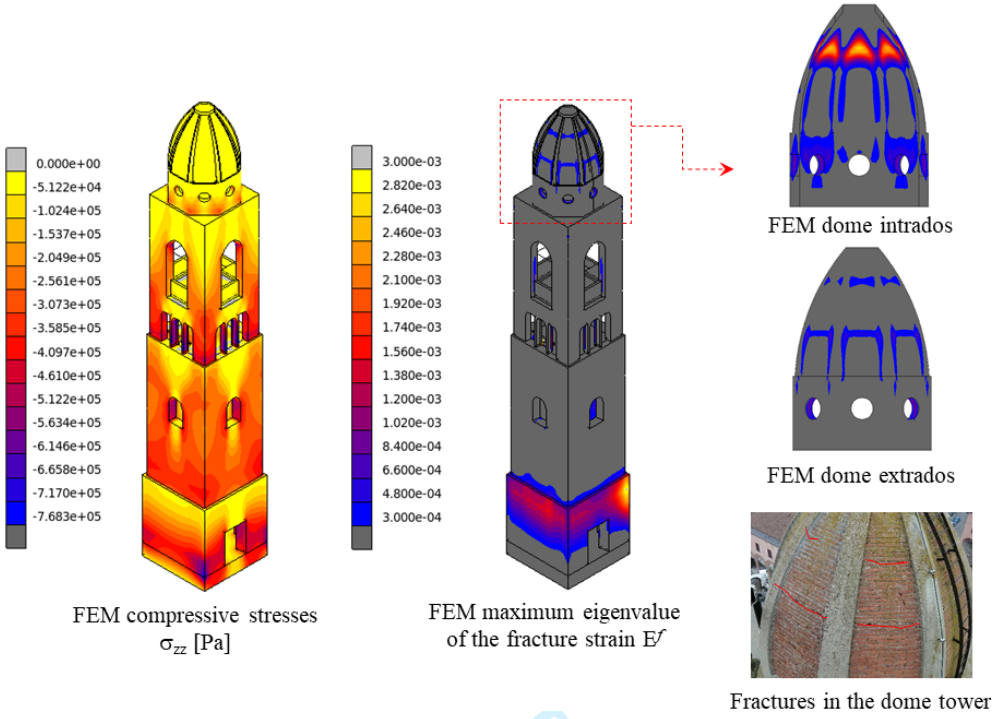

Figure 19. Numerical results of nonlinear static analysis for gravitational load: compressive stresses σ_{zz} (left); maximum eigenvalue of the fracture strain E^f (right).

Afterward, some dynamic analyses with time integration are performed, using the $H(t)$ force applied along the y direction, both in linear and nonlinear cases. Function $H(t)$, evaluated for $\alpha = 90°$ and $c = 0.79$, is plotted in Figure 18. The damping matrix has been calculated according to the Rayleigh hypothesis, using the experimental damping ratios estimated for the first two frequencies in Experiment 0 and reported in Table 3.
A comparison between experimental and numerical results is provided in Figure 20. Figure 20a shows the maximum velocities in the y-direction plotted versus the tower's height, achieved through the dynamic analyses (dashed grey line for the linear case and continuous green line for the nonlinear case); the experimental results are indicated by orange squares. Figure 20b reports the Fast Fourier Transform of the velocities recorded by sensor SS20 0943 and their numerical counterparts.
The analysis of the figure allows making the following observations:

- the numerical models overestimate the maximum velocity values compared to the experimental ones, with particular regard to the upper portions of the structure; it is worth noting, however, that the upper bell chamber's model, whose bending stiffness is substantially different from that of the tower's frame, is affected by numerous uncertainties regarding the actual geometry of the iron structure supporting the bells' system and the constituents materials of the masonry pillars;

- the linear and nonlinear numerical results are practically coincident, thus suggesting that the tower does not enter the nonlinear field as an effect of the bell's oscillations; the results

of the two analyses slightly differ in the tower portion between 18 and 24 m, corresponding to the upper bell chamber.

- both experimental and numerical results are characterized by a frequency response in the interval [1.9, 2.0] Hz, which also contains the first two natural frequencies of the tower. In addition, the numerical results show a predominant frequency of about 2.7 Hz, which also appears in the plot of the FFT of $H(t)$ in Figure 17.

It should be noted that the expression of $H(t)$ suggested by the technical rules [15] depends on many unknown parameters, all characterized by a high degree of uncertainty. At the same, time the choice of $H(t)$ strongly influences the dynamic response of the numerical model. The results obtained in this paper show that by adopting the approach proposed in [15] and appropriately choosing the unknown parameters, the numerical model can capture some relevant characteristics of the dynamic behaviour of the tower. In particular, the numerical maximum velocities at selected points along the tower are substantially in good agreement with their experimental counterparts. These encouraging preliminary results underscore the importance of combining experimental tests and numerical simulations while investigating the influence of parameter uncertainties on the dynamic response of the FE model.

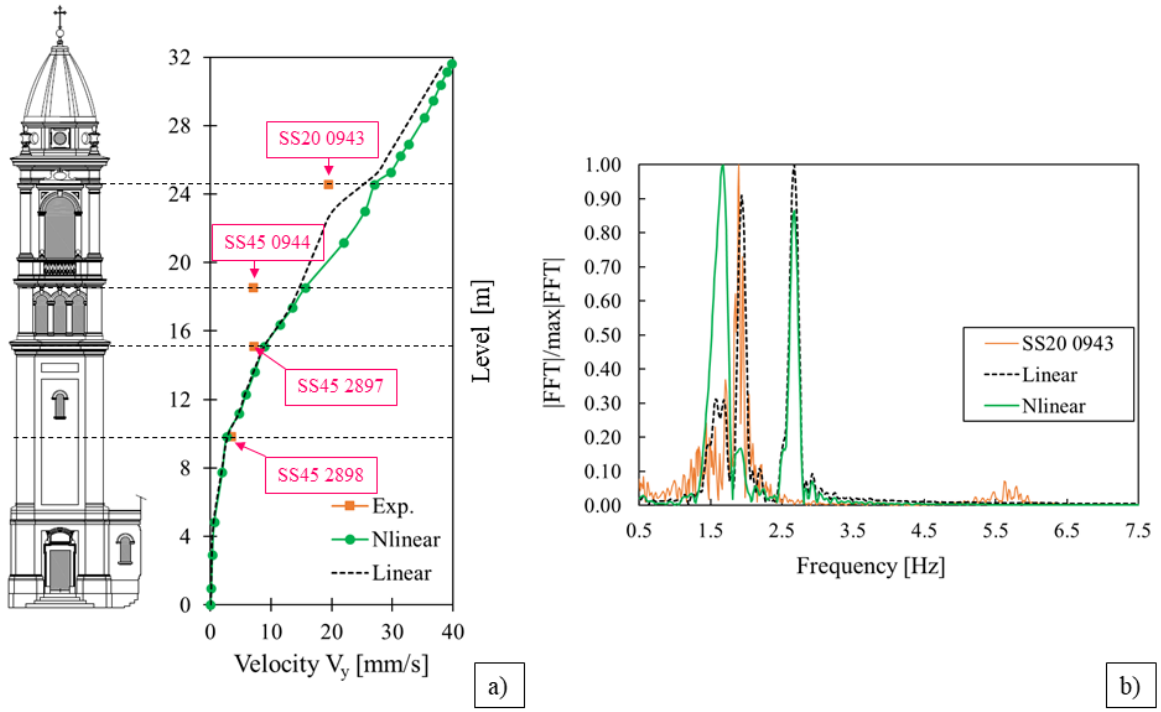

Figure 20. a) Maximum velocities at selected point along the height (the experimental values are in orange, the numerical values are represented by the continuous green line in the nonlinear case and the dashed black line in the linear case). B) FFT of the velocities recorded by the velocimeter SS20 0943 (orange line) and the numerical velocities in the linear case (dashed black line) and nonlinear case (green line).

5. CONCLUSIONS

This paper describes the investigations conducted on the tower of the Santissimo Crocifisso Sanctuary in Castel San Pietro, aimed at assessing the effects of the swinging bells on the structure's dynamic behaviour. The structure, featuring a carillon with fifty-five bells of different sizes, has been subjected

to a careful, complex monitoring campaign consisting of six experiments in which the bells have been selectively activated, complemented by two ambient vibration tests.
The primary outcomes of the experimental campaign can be summarized as follows.

1. The carillon's sound, modelled as an impulsive action on the tower, induces velocities in the order of 0.5 mm/s, both in the *x* and *y*-direction.
2. Experiments in which the bells in the upper chamber swing produce the highest velocity values in the swinging *y*-direction. These values are more significant than those induced by the carillon alone.
3. The most robust action is induced on the tower when all the bells (carillon plus swinging bells) ring. The highest measured values are located over the vault overlooking the upper bell chamber and reach 30 mm/s.
4. Swinging of the only bell no. 54 gives velocity values (up to 20 mm/s) comparable with those induced by all the bells playing.
5. The carillon's sound induces velocities that vary linearly with the tower's height.
6. The velocities induced by the swinging bells have a linear trend alongside the tower up to the bell chamber's floor (18 m), with values in the limit of 8 mm/s. Robust amplification of the velocity is shown in the tower's upper portions.

The FE numerical simulations conducted on the tower via the NOSA-ITACA code encompasse a preliminary calibration of the tower model and dynamic analyses of the structure subjected to the action of the heaviest swinging bell. The results of numerical simulation are affected by the assumptions made for the structure supporting the bells, whose geometry and characteristics are not adequately known, and by several uncertainties regarding the action of the swinging bell and then the expression of the time-dependent load $H(t)$. Despite these uncertainties, the numerical results, in terms of maximum velocities calculated at some selected points, are in reasonable agreement with the experimental ones. In addition, a comparison between the results of a linear and a no linear analysis, the latter conducted by modelling the masonry constituting the tower as a masonry-like material, shows that the tower behaves linearly under the action of the swinging bell. The preliminary dynamic analysis conducted in this paper is the first step towards accurate numerical modelling, which considers the numerous unknown parameters influencing the tower's response to time-dependent loads.

Acknowledgements

This research has been partially supported by the Fondazione Cassa di Risparmio di Lucca (SOUL project, 2019-2022). This support is gratefully acknowledged. The authors wish to thank Michele Naldi, Stelio Montebugnoli, Gilberto Dallavalle and Giada Gasperini for the technical support in the experimental campaign.

References

[1] Heyman J, Threlfall BD. Inertia forces due to bell-ringing. *Int J Mech Sci.* 1976;18(4):161-164. doi:10.1016/0020-7403(76)90020-5.
[2] Selby A.R. and Wilson J.M. The dynamics of masonry bell towers. *Computational Modelling of Masonry, Brickwork and Blockwork Structures.* 2001 Bull J.W. (Editor), Saxe-Coburg Publications.
[3] Bennati S, Nardini L, Salvatore W. Dynamic Behavior of a Medieval Masonry Bell Tower. Part I: Experimental Measurements and Modeling of Bell's Dynamic Actions. *J Struct Eng.* 2005;131(11):1647-1655. doi:10.1061/(asce)0733-9445(2005)131:11(1647)
[4] Bennati S, Nardini L, Salvatore W. Dynamic Behavior of a Medieval Masonry Bell Tower. II: Measurement and Modeling of the Tower Motion. *J Struct Eng.* 2005;131(11):1656-1664. doi:10.1061/(ASCE)0733-9445(2005)131:11(1656)

[5] Ivorra S, Pallarés FJ. Dynamic investigations on a masonry bell tower. *Eng Struct.* 2006;28(5):660-667. doi:10.1016/j.engstruct.2005.09.019
[6] Lepidi M, Gattulli V, Foti D. Swinging-bell resonances and their cancellation identified by dynamical testing in a modern bell tower. *Eng Struct.* 2009;31(7):1486-1500. doi:10.1016/j.engstruct.2009.02.014
[7] Ivorra S, Pallarés FJ, Adam JM. Dynamic behaviour of a modern bell tower - A case study. *Eng Struct.* 2009;31(5):1085-1092. doi:10.1016/j.engstruct.2009.01.002
[8] Casciati, S., Al-Saleh, R. Dynamic behavior of a masonry civic belfry under operational conditions. *Acta Mechanica*. 2020:215(1):211-224.
[9] Ivorra S, Foti D, Diafero M, Vacca V, Bru D. Resonances detected on a historical tower under bells' forced vibrations. *Frat ed Integrità Strutt.* 2018;12(46):203-215. doi:10.3221/IGF-ESIS.46.19
[10] Ivorra S, Pallarés FJ, Adam JM. Masonry bell towers: dynamic considerations. *Proc Inst Civ Eng - Struct Build.* 2011;164(1):3-12. doi:10.1680/stbu.9.00030
[11] Bru D, Ivorra S, Betti M, Adam JM, Bartoli G. Parametric dynamic interaction assessment between bells and supporting slender masonry tower. *Mech Syst Signal Process.* 2019;129:235-249. doi:10.1016/j.ymssp.2019.04.038
[12] Vincenzi L, Bassoli E, Ponsi F, Castagnetti C, Mancini F. Dynamic monitoring and evaluation of bell ringing effects for the structural assessment of a masonry bell tower. *J Civ Struct Heal Monit.* 2019;9(4):439-458. doi:10.1007/s13349-019-00344-9
[13] Tomaszewska A, Drozdowska M, Szymczak C. Vibration-Based Investigation of a Historic Bell Tower to Understand the Occurrence of Damage. *Int J Archit Herit*. Published online 2020. doi:10.1080/15583058.2020.1864511.
[14] Nochebuena-Mora E, Mendes N, Lourenço PB, Greco F. Dynamic behavior of a masonry bell tower subjected to actions caused by bell swinging. Structures. 2021;34:1798-1810. doi:10.1016/j.istruc.2021.08.066
[15] DIN 4178. *Glockentuerme, Berechnung und Ausfuehrung*, 1978.
[16] Ivorra S, Palomo MJ, Verdú G, Zasso A. Dynamic forces produced by swinging bells. *Meccanica.* 2006;41(1):47-62. doi:10.1007/s11012-005-7973-y
[17] DIN 4150-3. *Vibrations in buildings. Part 3: Effects on structures*, 1986.
[18] UNI 9916:2014, *Criteria for the measurement of vibrations and the assessment of their effects on buildings*, 2014.
[19] Brincker R, Ventura CE. *Introduction to Operational Modal Analysis.* Wiley Blackwell; 2015. doi:10.1002/9781118535141.
[20] Reynders E, Schevenels M and De Roeck G. *MACEC 3.4. The Matlab toolbox for experimental and operational modal analysis.* 2021 http://bwk.kuleuven.be/bwm/macec/.
[21] Pappa RS, Elliott KB, Schenk A. Consistent-mode indicator for the eigensystem realization algorithm. *J Guid Control Dyn.* 1993;16(5):852-858. doi:10.2514/3.21092.
[22] Masciotta MG, Pellegrini D. Tracking the variation of complex mode shapes for damage quantification and localization in structural systems. *Mech Syst Signal Process.* 2022;169:108731. doi:10.1016/j.ymssp.2021.108731
[23] Girardi M, Padovani C, Pellegrini D, Robol L. A finite element model updating method based on global optimization. *Mech Syst Signal Process.* 2021;152:107372. doi:10.1016/j.ymssp.2020.107372.
[24] Pianosi F, Sarrazin F, Wagener T. A Matlab toolbox for Global Sensitivity Analysis. *Environ Model Softw.* 2015;70:80-85. doi:10.1016/j.envsoft.2015.04.009
[25] Morris MD. Factorial Sampling Plans for Preliminary Computational Experiments. *Technometrics*. 1991;33(2):161. doi:10.2307/1269043
[26] McKay MD, Beckman RJ, Conover WJ. A Comparison of Three Methods for Selecting Values of Input Variables in the Analysis of Output from a Computer Code. *Technometrics.* 1979;21(2):239. doi:10.2307/1268522.
[27] Lucchesi M, Zani N, Padovani C, Pasquinelli G. *Masonry Constructions: Mechanical Models and Numerical Applications*. Vol 39. Springer Berlin Heidelberg; 2008. doi:10.1007/978-3-540-79111-9
[28] Manuale dell'Architetto CNR, Italy 1986 (in Italian).